Journal of Applied Electrochemistry **29**: 919–926, 1999.
© 1999 *Kluwer Academic Publishers. Printed in the Netherlands.*

Cyclone flow cell for the investigation of gas-diffusion electrodes

K. SUNDMACHER
Institut für Chemische Verfahrenstechnik, Technische Universität Clausthal, Leibnizstrasse 17, D-38678 Clausthal-Zellerfeld, Germany
(address for correspondence: Max-Planck-Institute for Dynamics of Complex Technical Systems, Leipziger Strasse 44, ZENIT-Building, D-39120 Magdeburg, Germany; e-mail: sundmacher@mpi-magdeburg.mpg.de)

Received 6 March 1998; accepted in revised form 8 December 1998

Key words: cell design, gas-diffusion electrodes, gas–liquid reactions, limiting current technique, mass transfer

Abstract

Electrochemical gas–liquid reactions can be efficiently carried out at porous gas diffusion electrodes (GDE). These electrodes are simultaneously in contact with a gas phase and a liquid phase. For the design and scale-up of electrochemical reactors based on these GDE their macrokinetic behaviour (i.e., the interaction of reaction and internal mass transport phenomena) must be investigated under well defined external mass transfer conditions and controlled wetting conditions. To meet these requirements, a novel cyclone cell has been designed in which two vortex flow fields are realised on either side of a horizontally positioned GDE. The external mass transfer coefficients in this cell are determined from limiting current measurements for the oxidation of $Fe(CN_6)^{4-}$.

List of symbols

A^S	electrode area exposed to the liquid phase (m^2)
Ba	Debye–Hückel parameter $(kg\ mol^{-1})^{1/2}$
$c^{G,L}$	molar gas bulk or liquid bulk concentration of A_1 ($mol\ m^{-3}$)
$c_0^{G,L}$	molar concentration of A_1 at gas or liquid inlet ($mol\ m^{-3}$)
c_i^L	molar concentration of ion i ($mol\ m^{-3}$)
c_t^L	total molar concentration of mixture ($mol\ m^{-3}$)
c_w^L	molar water concentration ($mol\ m^{-3}$)
D^L	liquid phase Fickian diffusion coefficient of salt ($m^2\ s^{-1}$)
$\mathscr{D}^L$	liquid phase diffusion coefficient of salt based on chemical potential gradient ($m^2\ s^{-1}$)
$\mathscr{D}_{i,w}^L$	ion-water Maxwell–Stefan diffusivity ($m^2\ s^{-1}$)
F	Faraday's constant ($= 96\,485\ C\ mol^{-1}$)
h	gap below cyclone inner tube (m)
I_m	molal ionic strength ($mol\ kg^{-1}$)
i_{lim}	limiting current density ($A\ m^{-2}$)
k^L	liquid phase mass transfer coefficient ($m\ s^{-1}$)
m	molal concentration ($mol\ kg^{-1}$)
R	electrode radius (m)
Re	Reynolds number ($\equiv \omega R^2 \rho \mu^{-1}$)
Sc	Schmidt number ($\equiv \mu \rho^{-1} (D^L)^{-1}$)
Sh	Sherwood number ($\equiv k^L R (D^L)^{-1}$)
t_-	anion transference number
$\dot{V}$	volumetric flow rate ($dm^3\ min^{-1}$)
v	resulting fluid velocity at the electrode radius ($m\ s^{-1}$)
$z_{+,-}$	charge numbers of cation or anion ($z_+ = 1, z_- = -4$)

Greek letters

α	Debye–Hückel constant $(kg\ mol^{-1})^{1/2}$
$\gamma_\pm$	mean molal activity coefficient
δ	thickness of hydrodynamic boundary layer (m)
μ	dynamic viscosity of fluid (Pa s)
ρ	mass density of fluid ($kg\ m^{-3}$)
ω	angular velocity (s^{-1})

Superscripts

G, L	gas bulk, liquid bulk
∞	at infinite dilution in water

Subscripts

$+$	related to cation, here: K^+
$-$	related to anion, here: $Fe(CN)_6^{4-}$

1. Introduction

Porous gas-diffusion electrodes (GDE) have been successfully used in a number of technical applications such as the production of electrical energy, as energy saving counter electrodes, for the generation of substances like hydrogen peroxide and for gas purification processes [1, 2]. For the design and scale-up of any electrochemical equipment based on GDE there is a need for reliable and reproducible kinetic data. Such kinetic information should be obtained from polarization measurements at a small area of a GDE which is exposed to a well defined flow field.

For the analysis of reaction and transport phenomena at planar electrodes, the use of rotating disc electrodes (RDE) is common and well understood [3]. By controlled rotation of the electrode in a stationary fluid, a defined flow field at the electrode surface is generated. However, this experimental technique is not directly applicable to a GDE in whose porous structure a gaseous reactant and a liquid electrolyte are brought into contact from opposite sides. Thus, two flow fields, on the gas side and on the liquid side, have to be realized. Therefore a new standard electrochemical cell has to be developed which is suitable for the characterization of GDE under technically relevant conditions.

2. Design of a cyclone flow cell

If a cell is to be suitable to obtain kinetic information from a GDE, well-defined flow fields with constant thicknesses of the external diffusion layers on both sides of the electrode are required. Furthermore, to achieve a uniform penetration of the electrolyte into the GDE pore structure, the electrode should be horizontal. For the evaluation of the observed reaction rates it is convenient to have a cell with small conversions, i.e. inlet and outlet concentration have nearly the same values. This is fulfilled if, at given gas and liquid flow rates $\dot{V}^{G,L}$, the external electrode area A^S is sufficiently small:

$$c^{G,L} = \frac{c_0^{G,L}}{1 + A^S k^{G,L}/\dot{V}^{G,L}} \approx c^{G,L} \quad \text{if } \frac{A^S k^{G,L}}{\dot{V}^{G,L}} \ll 1 \qquad (1)$$

2.1. *Vortex flow field*

In the conventional rotating disc electrode arrangement, the rotational flow field leads to a hydrodynamic boundary layer of constant thickness δ_{RDE} over the electrode surface. For laminar conditions the thickness is given by [4]

$$\delta_{RDE} = 4\left(\frac{\mu}{\rho\omega}\right)^{1/2} \qquad (2)$$

In Equation 2 δ_{RDE} is defined as the distance for which the deviation of the peripheral velocity is 2%. Similar conditions would be achieved at both surfaces of a GDE if the fluid were rotated over a stationary electrode, instead of the electrode rotating in a stationary fluid. Vortex flow with constant angular velocity ω over an infinite surface has been the subject of extensive theoretical investigation [4]. This flow field is depicted in Figure 1.

Bödewadt [5] and Nydahl [6] solved the Navier–Stokes equations for the laminar vortex flow. These authors found that the thickness of the hydrodynamic boundary layer δ_{vortex} is also constant for this arrangement and is twice δ_{RDE}:

$$\delta_{vortex} = 8\left(\frac{\mu}{\rho\omega}\right)^{1/2} \qquad (3)$$

An established method of generating a vortex flow field is the use of vertical axis impeller with flat radially oriented blades. A vortex flow can also be realised in a cyclone, the main advantages being the simple cone design and the avoidance of moving parts. The fluid is tangentially introduced at the upper edge of the cone and follows a circular path towards the cone end. For reasons of continuity, the fluid rises in the middle of the cone and is removed by an inner tube. Figure 2

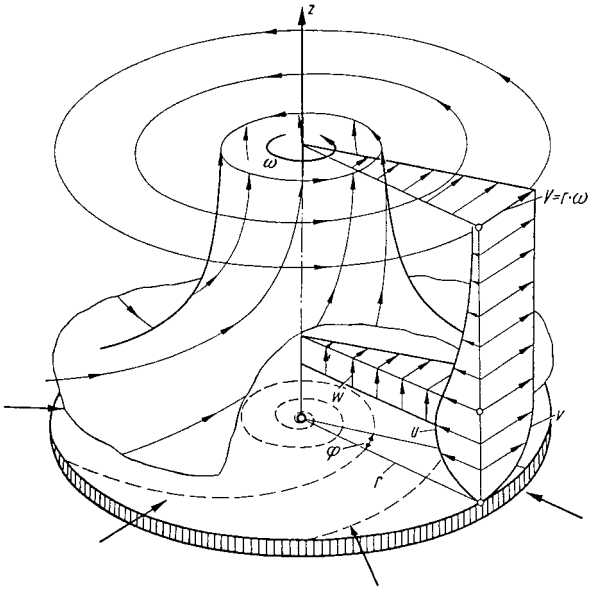

Fig. 1. Vortex flow field above a stationary surface (adopted from [4]); velocities: u = radial (v_r), v = tangential (v_φ), w = axial (v_z).

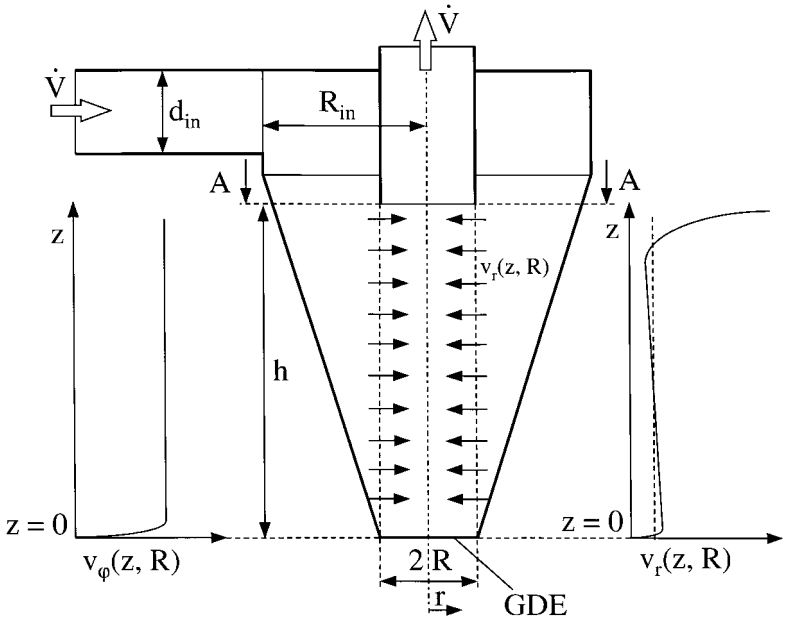

Fig. 2. Schematic of a cyclone; profiles of tangential and radial velocities at the inner tube, $\dot{V}$: flow rate (e.g., see [7]), for cut A–A see Figure 3.

demonstrates the principle of the cyclone with illustrative velocity profiles.

The flow in a cyclone can be approximately described as a potential vortex. Due to friction at the cone walls and at the inner tube, the rotational momentum of the flow is reduced. In addition, turbulence is introduced at the fluid inlet. These phenomena make it difficult to predict the flow field purely theoretically. Despite this disadvantage, the cyclone generates a well defined flow field and is therefore a useful tool for the electrochemical characterization of a GDE.

The design parameters are the height of the cyclone, the cone angle and the dimensions of the inner tube. The dimension of the small cone end depends on the electrode surface area. To limit the maximum electrical current, an area of $A^{S} = 2\,\mathrm{cm}^2$ was used. A cone angle of 20° was chosen in order to reduce the pressure drop in the fluid and to provide sufficient space for external tube connection.

2.2. *Definition of Reynolds number*

The Reynolds number, *Re*, is defined using the fluid velocity v at the radius of the inner tube R (identical to the electrode radius). This velocity is composed of the tangential velocity component, v_φ, and the radial velocity component, v_r (see Figure 3):

$$Re \equiv \frac{vR\rho}{\mu} \quad \text{with} \quad v = \sqrt{v_\varphi(0,R)^2 + v_r(0,R)^2} \tag{4}$$

The two velocity components are expressed in terms of the known flow rate $\dot{V}$. For $r > R$, the radial profile of the tangential velocity component v_φ can be approximated by the relation [7]

$$v_\varphi r^{1/2} = \text{const.} \tag{5}$$

According to Barth [8] the tangential velocity at the inner tube radius $v_\varphi(z,R)$ is nearly constant along the axial coordinate z. Therefore, using Equation 5, the tangential velocity at the electrode surface $v_\varphi(0,R)$ can be estimated from the tangential velocity at the cyclone inlet $v_{\varphi,\mathrm{in}}$:

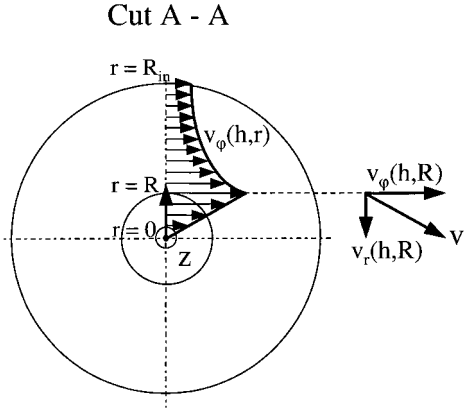

Fig. 3. Left: profile of tangential velocity v_φ against radial coordinate; right: resulting velocity v at the electrode radius.

$$v_\varphi(0,R) = \left(\frac{R_{in}}{R}\right)^{1/2} v_\varphi(0,R_{in}) \quad \text{with}$$

$$v_\varphi(0,R_{in}) = v_{\varphi,in} = \frac{4\dot{V}}{\pi d_{in}^2} \tag{6}$$

where R_{in} stands for the cyclone radius at the middle of the inlet tube (here: $R_{in} = 29.7$ mm), R stands for the radius of the free electrode area (here: $R = 8$ mm), and d_{in} is the diameter of the inlet tube (here: $d_{in} = 4$ mm).

The radial velocity component, v_r, at the electrode radius is given by

$$v_r(z,R) = \frac{\dot{V}}{2\pi R h} \tag{7}$$

Equation 7 is based on the assumption of Barth [8] that the radial velocity component v_r does not vary significantly along the cyclone height. This is only an approximation because in the gap below the inner tube v_r can have very high values and varies along the cyclone axis [9]. For the ratio of the two velocities,

$$\frac{v_\varphi(0,R)}{v_r(0,R)} = 8\frac{h\sqrt{R_{in}R}}{d_{in}^2} \tag{8}$$

With the given dimensions and a gap of $h = 10$ mm, the velocity ratio $v_\varphi(0,R)/v_r(0,R) = 77$ is predicted from Equation 8. Therefore, the radial component of the resulting vector is negligible in comparison to the tangential component and for the Reynolds number the simplified definition

$$Re \equiv \frac{v_\varphi(0,R)R\rho}{\mu} = \frac{\omega R^2 \rho}{\mu} \tag{9}$$

will be used. Equation 9 corresponds to the definition which is used for a RDE [3]. Equation 6 gives the angular velocity ω in the cyclone cell

$$\omega = \frac{v_\varphi(0,R)}{R} = \frac{4R_{in}^{1/2}}{\pi R^{3/2} d_{in}^2}\dot{V} \tag{10}$$

Based on the dimensions of the cyclone flow cell the relation

$$\frac{\omega}{(s^{-1})} = 320\frac{\dot{V}}{(dm^3\,min^{-1})} \tag{11}$$

is obtained. For flow rates between $\dot{V} = 1.0$ dm^3 min^{-1} and 10 dm^3 min^{-1} angular velocities between $\omega =$ 300 min^{-1} and 3000 min^{-1} are achieved. For comparison, a conventional RDE usually rotates with velocities between $\omega = 100$ min^{-1} and 10 000 min^{-1} [3]. The laminar–turbulent transition at a RDE was found to take place above the critical Reynolds number $Re_{crit,RDE} \approx 2 \times 10^5$. For the cyclone flow cell the critical number was found to be considerably lower i.e. $Re_{crit,cyclone} \approx 10^3$. This is due to the fact that a boundary layer is formed along the cyclone wall so that the effective length for fluid-wall friction is longer than the electrode radius R which is applied in the Reynolds number definition.

2.3. *Cyclone flow cell and its operation*

The complete cyclone flow cell is presented in Figure 4. The cell consists of an upper compartment for the liquid phase and a lower compartment for the gas phase. On the electrolyte side of the cell a Luggin capillary is provided which is connected to a cylindrical vessel containing the reference electrode (Ag/AgCl in 3 M KCl). Using this arrangement the reference electrode is close to the working electrode with no interference with the electrostatic field in the liquid compartment. The vortex flow inside the electrolyte compartment generates an overpressure. This can lead to an undesirable flow of

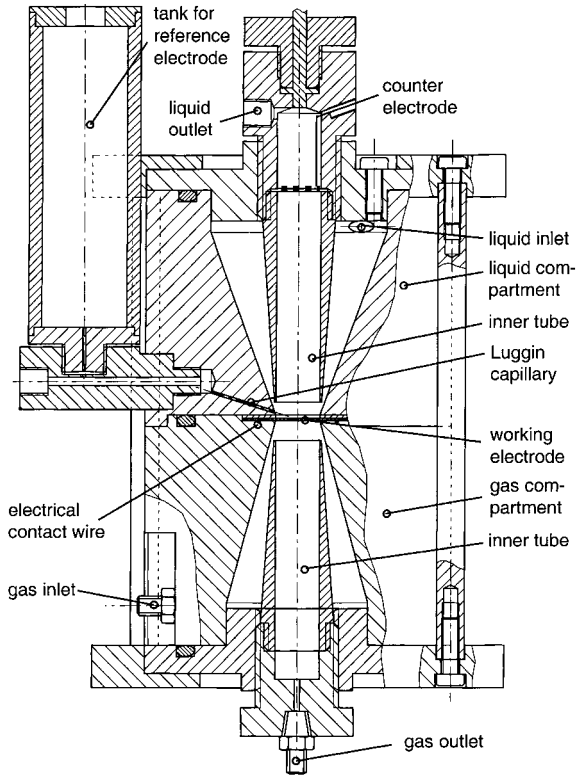

Fig. 4. Design of the cyclone flow cell.

electrolyte liquid through the capillary. However, this flow can be suppressed by means of a flow resistance located inside the capillary. The counter electrode (platinum mesh) is located inside the liquid outlet tube. It is oriented parallel to the working electrode and has almost the same external area. The gaps between the working electrode and the inner tubes are adjustable. The cell parts are fastened by two stainless steel rings and six stainless steel screws. Electrical contact to the working electrode is made by a tantalum wire. The experimental set-up, including the flow cell and its peripherals, is shown in Figure 5.

3. Determination of mass transfer coefficient

The mass transfer coefficient k^L at the surface of an electrode can be determined from the limiting current i_{lim}. As a model reaction, the oxidation of ferricyanide(II) at a smooth graphite electrode was chosen:

$$Fe(CN)_6^{4-} \rightarrow Fe(CN)_6^{3-} + e^-, \quad \text{Counterion: } K^+ \quad (12)$$

Under limiting current conditions the concentration of ferricyanide(II) at the electrode surface drops to zero and the mass transfer coefficient k^L can be calculated from

$$k^L = \frac{i_{lim}}{Fc_-^L} \quad (13)$$

The potentiostatic measurements were carried out with a computer controlled potentiostat PC3/750 (Gamry Instruments) in the potential region from 0.2 to 1.5 V vs NHE in steps of 50 mV. Each experiment was performed twice and, for determination of mass transfer coefficients, averaged data were used. The ohmic potential drop between the working and the reference electrode was determined by application of the current interruption technique [10].

3.1. *Experimental results*

Figure 6 shows polarization data from two successive runs. The mass transfer limitation becomes dominant above $U = 1.2$ V vs NHE and a limiting current of $i_{lim} = 21.0$ mA cm^{-2} is achieved. Above $U = 1.5$ V a significant increase in cell current is observed due to anodic oxygen evolution. Experiments revealed that the use of an inner tube with a gap of $h = 10$ mm leads to an increase in limiting current by 20% compared to the arrangement without an inner tube. However, the reproducibility of polarization data was less satisfactory when an inner tube was used. For this reason, in the following, no inner tube was installed.

As an example Figure 7 shows polarization curves from the cyclone flow cell for five different flow rates between $\dot{V}^L = 0.4$ and 1.2 dm^3 min^{-1} at the same bulk concentration of ferricyanide(II). As expected, the limiting current increases with flow rate. A series of polarization experiments within the concentration range

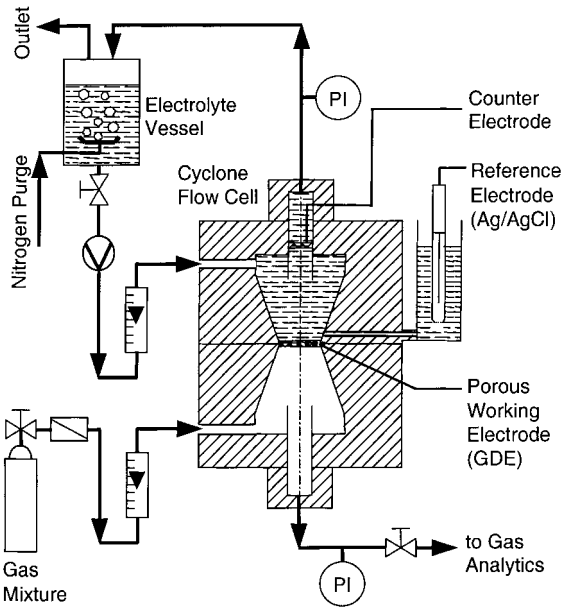

Fig. 5. Schematic of the experimental set-up.

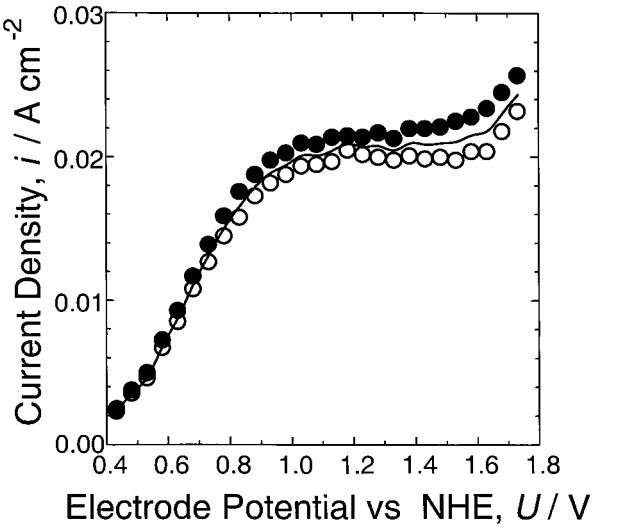

Fig. 6. Two successive experimental potentiostatic polarization curves for the oxidation of ferricyanide(II) at a graphite electrode in the cyclone flow cell. Conditions: $T = 25\,^\circ$C; without inner tube; liquid flow rate $\dot{V}^L = 1.0$ dm^3 min^{-1}; molality $m^L = 0.1$ mol kg^{-1}. Key: (○) first measurement, (●) second measurement, (—) averaged.

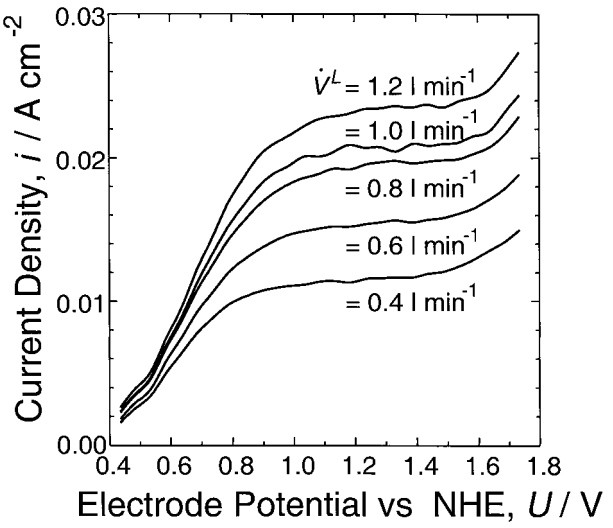

Fig. 7. Experimental potentiostatic polarization curves for the oxidation of ferricyanide(II) at a graphite electrode in the cyclone flow cell for five different liquid flow rates: $\dot{V}^{L}$ with $T = 25\,^{\circ}\mathrm{C}$; without inner tube; molality $m^{L} = 0.1$ mol kg^{-1}.

between $m^{L} = 0.005$ and 0.10 mol kg^{-1} was performed at constant flow conditions ($\dot{V}^{L} = 0.8$ dm^3 min^{-1}). The mass transfer coefficient k^{L} depends significantly on the concentration of the active species (see Figure 8). This has to be considered in the evaluation of the experimental data.

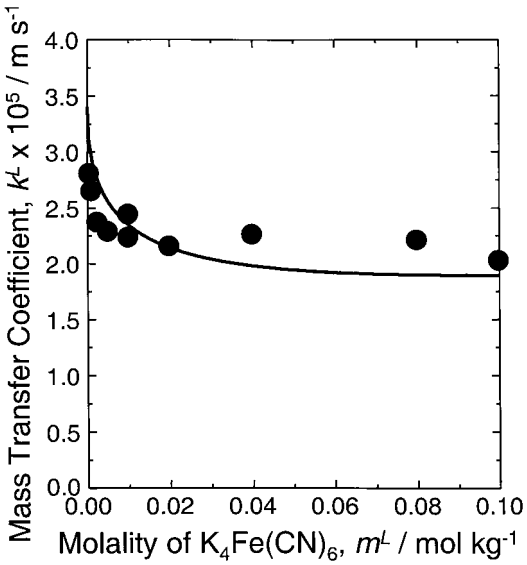

Fig. 8. Dependence of mass transfer coefficient on the molal concentration of potassium hexaferricyanide(II). Key: (●) experimental data with $T = 25\,^{\circ}\mathrm{C}$; without inner tube; liquid flow rate $\dot{V}^{L} = 0.8$ dm^3 min^{-1}; (—) calculated from Equation 19 with $Ba = 1$ (kg mol^{-1})$^{1/2}$ and $k^{L\infty} = 3.4 \times 10^{-5}$ m s^{-1}.

3.2. *Dependence of mass transfer coefficient on concentration*

The main reason for the observed variability of mass transfer coefficients at constant flow conditions lies in the dependence of the diffusivities on the mixture composition. According to Newman [11a] the Fickian diffusion coefficient D^{L} in a concentrated solution of a binary salt can be calculated from

$$D^{L} = \mathscr{D}^{L}\frac{c_{t}^{L}}{c_{w}^{L}}\left(1 + \frac{\partial \ln \gamma_{\pm}}{\partial \ln m^{L}}\bigg|_{T}\right) \tag{14}$$

where the diffusion coefficient $\mathscr{D}^{L}$ is based on the chemical potential gradient as the real thermodynamic driving force of the diffusional transport. This coefficient is related to the ion-water Maxwell–Stefan diffusivities $Đ^{L}_{+,w}$ and $Đ^{L}_{-,w}$ by [11b]

$$\mathscr{D}^{L} = \frac{Đ^{L}_{+,w}Đ^{L}_{-,w}\,(z_{+} - z_{-})}{z_{+}Đ^{L}_{+,w} - z_{-}Đ^{L}_{-,w}} \tag{15}$$

The ion-water diffusivities are fairly independent of concentration and can be approximated by the diffusion coefficients at infinite dilution of ions in water [12]. In the case of potassium ferricyanide(II) these coefficients are (at $T = 25\,^{\circ}\mathrm{C}$ [11c]):

$$Đ^{L}_{+,w} \approx Đ^{L\infty}_{+,w} = 1.957 \times 10^{-9}\ \mathrm{m^2\,s^{-1}},$$
$$Đ^{L}_{-,w} \approx Đ^{L\infty}_{-,w} = 0.739 \times 10^{-9}\ \mathrm{m^2\,s^{-1}}$$

Equation 15 yields the following diffusion coefficient for the salt: $\mathscr{D}^{L} = 1.472 \times 10^{-9}$ m^2 s^{-1}. For moderately dilute solutions the mean molal activity coefficient $\gamma_{\pm}$ in Equation 14 can be predicted by the Debye–Hückel theory [11d]:

$$\ln \gamma_{\pm} = \frac{z_{+}z_{-}\alpha\sqrt{I_{m}}}{1 + Ba\sqrt{I_{m}}} \tag{16a}$$

with

$$I_{m} \equiv \frac{1}{2}\sum_{i=1}^{N} m_{i}^{L} z_{i}^{2} \tag{16b}$$

where the constant α depends on the nature of the solvent ($\alpha = 1.173$ (kg mol^{-1})$^{1/2}$ in water at 25 °C), the parameter Ba depends on the ion radius, and the molal ionic strength is $I_{m} = 10\,m^{L}$ for potassium ferricyanide(II). By differentiating Equation 16a with respect to the molality m^{L} and combining the result with Equation

14, the diffusivity of the considered component in water is obtained:

$$D^{\mathrm{L}} = \mathscr{D}^{\mathrm{L}} \left(1 - \frac{7.4\sqrt{m^{\mathrm{L}}/(\mathrm{mol\,kg^{-1}})}}{\left(1 + Ba\sqrt{10\ m^{\mathrm{L}}}\right)^2} \right) \tag{17}$$

where the total mixture concentration $c_{\mathrm{t}}^{\mathrm{L}}$ is approximated by the water concentration, $c_{\mathrm{t}}^{\mathrm{L}} \approx c_{\mathrm{w}}^{\mathrm{L}} = 55.56$ mol dm^{-3} which is justified for the present experiments ($m^{\mathrm{L}} < 0.1$ mol kg^{-1}). From laminar boundary layer theory, the following dependence of the mass transfer coefficient k^{L} on the Fickian diffusivity D^{L} is known [13]:

$$k^{\mathrm{L}} \propto (D^{\mathrm{L}})^{2/3} \tag{18}$$

Equation 18 in combination with Equation 17 gives

$$k^{\mathrm{L}} = k^{\mathrm{L}\infty} \left(1 - \frac{7.4\sqrt{m^{\mathrm{L}}/(\mathrm{mol\,kg^{-1}})}}{\left(1 + Ba\sqrt{10\ m^{\mathrm{L}}}\right)^2} \right)^{2/3} \tag{19}$$

Newman [11c] recommends the use of $Ba = 1.0$ (kg mol^{-1})$^{1/2}$ for all types of electrolytes. The only remaining parameter to be determined is the mass transfer coefficient at infinite dilution $k^{\mathrm{L}\infty}$. By extrapolation from the series of measurements at different dilutions (described in Section 3.1), $k^{\mathrm{L}\infty} = 3.4 \times 10^{-5}$ m s^{-1} was obtained. In Figure 8 the experimental data and their fit by Equation 19 are depicted. The quality of the fit is remarkably good, considering the fact that Equation 19 is based on laminar boundary layer theory although the flow in the cyclone cell is already turbulent at $Re > 10^3$.

3.3. *Dimensionless data correlation*

Levich [13] originally derived an analytical solution for ion deposition at a RDE under laminar flow conditions. For the case of anion deposition the equation, rearranged in terms of the relevant dimensionless numbers, is

$$Sh = \frac{0.62}{1 - t_-} Re^{1/2}\ Sc^{1/3} \tag{20}$$

for

$$Re < 2 \times 10^5 \text{ and } Sc \geqslant 1.$$

The anion transference number t_- is given by

$$t_- = 1 - t_+ = \frac{-z_- \mathscr{D}_{-,\mathrm{w}}^{\mathrm{L}}}{z_+ \mathscr{D}_{+,\mathrm{w}}^{\mathrm{L}} + z_- \mathscr{D}_{-,\mathrm{w}}^{\mathrm{L}}} = 0.60 \tag{21}$$

In Equation 20 the first term on the right hand side accounts for the influence of migration. It can be seen that migration leads to a substantial increase in anion mass transfer by a factor of 2.5, a factor which is almost independent of concentration.

A similar correlation can be established for the mass transfer conditions in the cyclone flow cell. According to Equation 18 the dependence of *Sh* on *Sc* is the same as in Equation 20. But the *Re* influence will be different due to the turbulent flow regime. Therefore the following relation is used:

$$Sh = \frac{q_1}{1 - t_-} Re^{q_2}\ Sc^{1/3} \tag{22}$$

For the determination of the parameters q_1 and q_2 in Equation 22, it is convenient to plot the experimental data logarithmically (see Figure 9):

$$\log\left(\frac{Sh}{Sc^{1/3}}\right) = \log\frac{q_1}{1 - t_-} + q_2 \log\ Re \tag{23}$$

From a linear regression analysis the parameters $q_1 = 0.0136$ and $q_2 = 2/3$ are obtained. The correlation coefficient is $r = 0.9897$.

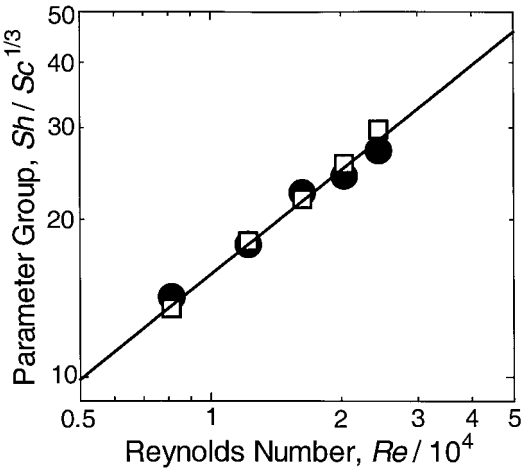

Fig. 9. Mass transfer coefficients correlated in terms of the dimensionless Sherwood, Reynolds and Schmidt numbers. Key: (●, □) experimental data ($T = 25\,^{\circ}$C; without inner tube); (—) Equation 23 with parameters $q_1 = 0.0136$ and $q_2 = 2/3$.

4. Conclusions

Porous GDE are applied for electrochemical gas–liquid reactions. The reactions are affected by the internal mass transfer resistances of the GDE pore structure. To obtain quantitative information on the internal mass transfer, it is necessary to investigate the electrode polarisation characteristics under well-defined external mass transfer conditions. Therefore, a double cyclone flow cell has been designed which provides vortex flow fields on both sides of the GDE. The external mass transfer from the cyclone liquid bulk to the electrode surface was investigated by limiting current technique at non-porous electrodes. Based on the experimental mass transfer coefficients the Sherwood correlation

$$Sh = \frac{0.0136}{1 - t_-} Re^{2/3}\, Sc^{1/3} \text{ (for } Re > 10^3 \text{ and } Sc \geqslant 1)$$

was formulated. The *Re* power, 2/3, confirms the existence of a turbulent flow regime at the electrode surface. As long as $Re > 10^3$, the mass transfer correlation is also applicable to estimate the external mass transfer coefficients on the gas side of a gas-diffusion electrode. This is justified because the flow cell was designed as a double cyclone with nearly the same geometries for the two compartments.

References

1. K. Sundmacher, *Reaktionstechnische Grundlagen der elektrochemischen Absorption mit Gasdiffusionselektroden*, VDI-Fortschrittbericht, Reihe 3, No. 564, VDI-Verlag, Düsseldorf. (1998).
2. K. Sundmacher and U. Hoffmann, *Chem. Eng. Sci.* **54** (1999) to appear.
3. A.J. Bard and L.R. Faulkner, *Electrochemical Methods – Fundamentals and Applications*, J. Wiley & Sons, New York (1980) pp. 283–98.
4. H. Schlichting, *Boundary-Layer Theory*, 7th edn, McGraw-Hill, New York (1987).
5. U.T. Bödewadt, *ZAMM* **20** (1940) pp. 241–53.
6. J.E. Nydahl, *Heat Transfer for the BÖDEWADT Problem*, Dissertation, Colorado State University, Fort Collins, CO. (1971).
7. K. Leschonski, *Mehrphasenströmungen II*, Lecture manuscript, TU Clausthal, (1986) sections 4.1–4.23.
8. W. Barth, *Brennstoff-Wärme-Kraft* **8** (1956) 1–9.
9. W. Krambrock, *Aufbereitungstechnik* **12** (1971) 391–401 and 643–49.
10. Gamry Instruments, Inc., *CMS 100 Framework Software*, *Operator's Manual*, CMS 105 DC Corrosion Test System, USA (1994) pp. 1–9.
11. J.S. Newman, *Electrochemical Systems*, 2nd edn, Prentice-Hall, NJ, (1991), a. 267–69, b. 253–56, c. 255, d. 97–101.
12. R. Krishna and J.A. Wesselingh, *Chem. Eng. Sci.* **52** (1997) 861–911.
13. B. Levich, *Acta Physicochimica URSS* **17** (1942) 257–307.